Time-varying Linear Reduced Order Model for Hypersonic Aerothermoelastic Analysis

Damien Guého*, Puneet Singla†, Daning Huang‡
Department of Aerospace Engineering, Pennsylvania State University, Univeristy Park, PA-16802

The coupled analysis between the flight dynamics, structural dynamics, heat transfer, and hypersonic aerothermodynamics, viz. AeroThermoServoElasticity (ATSE), is a key ingredient for evaluating the performance, stability, and reliability of hypersonic vehicles. A thorough performance analysis for ATSE is computationally intractable with high fidelity models for each discipline. Hence, there is a need to develop accurate reduced order models (ROM) for aerothermodynamics as well as thermoelasticity. This work exploits the latest advances in dynamic system theory to develop a reduced order model for aerothermoelastic analysis. The Time-Varying Eigensystem Realization Algorithm (TVERA) is used to identify a linear time varying (LTV) model from a high fidelity computational framework with guaranteed observability. The simulations performed show a good agreement between the reduced-order and high fidelity models.

I. Introduction

Air-breathing hypersonic vehicles are under increasingly active development in the recent years [1, 2]. This class of vehicles are expected to operate at high Mach number in the atmosphere for the entire mission profile that can last for 30 minutes or even longer time. Due to the high speeds, the vehicle is exposed to the extreme aerothermodynamic environment involving combined aero-thermo-acoustical loadings. The aerothermal loads are due to the hypersonic aerodynamic pressure and heat flux. The acoustical loads are inherently stochastic and mainly due to the strong turbulent interaction present in the hypersonic boundary layer over the complex vehicle geometry. The high heating rates lead to degradation of material properties. The thermal stresses introduced by the temperature gradients and geometrical constraints affect the structural integrity and cause structural instabilities, including buckling and flutter. The thermoelastic effect further impacts the controllability of the vehicle, esp. the response effectiveness of aerodynamic control surfaces. It is clear that the coupling between the structural dynamics, heat transfer, and hypersonic aerothermodynamics, viz. aerothermoelasticity, constitutes the core subsystem governing the operation of a hypersonic vehicle. The predictive aerothermoelastic capability over extended flight time is a key ingredient for analyzing performance, stability, and reliability of hypersonic vehicles.

However, due to the current limited capability of ground tests and the lack of available flight test data, there is a significant degree of uncertainty associated with the aerothermoelastic modeling of hypersonic vehicles and limited ability to alleviate this uncertainty through experimental testing [3]. Therefore, the aerothermoelastic analysis, as a high-dimensional nonlinear multi-physics problem spanning across multiple spatial and temporal scales, involves strong stochastic dynamics as well as model uncertainties that is due to either imperfect high-fidelity models or reduced-order models. The uncertainty propagate across the coupling interfaces between the models and aggregate over time in the aerothermoelastic analysis. While there is a large body of research conducted on the uncertainty quantification (UQ) of aeroelasticity and aerothermoelasticity, the studies either focused on the calibration of models of a single discipline [4–7], or the quantification of several parametric stochastic variables in coupled analysis [8, 9]. Significant algorithmic development is required to identify, quantify, and propagate these stochastic effects and model errors through a time-dependent, high-dimensional state space, as is the case for hypersonic aerothermoelastic analysis.

Currently, the aerothermoelastic analysis is typically carried out using a computationally efficient kriging-based aerothermal surrogate coupled to nonlinear finite element models for structural dynamics and heat transfer, i.e. the thermoelastic solver [10–12]. It is relatively easy to quantify and propagate the uncertainty associated with the

*PhD Candidate, Department of Aerospace Engineering, Pennsylvania State University, University Park, PA-16802, Email: djg76@psu.edu.
†Professor, AIAA Associate Fellow, AAS Fellow, Department of Aerospace Engineering, Pennsylvania State University, University Park, PA-16802, Email: psingla@psu.edu.
‡Assistant Professor, AIAA Member, Department of Aerospace Engineering, Pennsylvania State University, University Park, PA-16802, Email: daning@psu.edu.

aerothermal loads by exploiting the mathematical formulation for kriging [13]. However, uncertainty quantification and propagation in a nonlinear thermoelastic model is challenging in general. As a step towards the efficient uncertainty quantification in aerothermoelastic analysis, we propose to develop a new time-varying *linear* reduced-order model (ROM), via a system identification formalism, for the high-dimensional nonlinear thermoelastic solver in the conventional aerothermoelastic analysis. Once such a linear ROM becomes available, the UQ of aerothermoelastic analysis over extended time will become tractable. This paper uses an implementation of a time-varying version of the Eigensystem Realization Algorithm (ERA) in order to obtain this time-varying linear reduced-order model.

Since the mid-sixties the field of system identification has been an important discipline within the automatic control area, structural engineering, modal testing and the recent developments in the field of system identification provide effective and accurate analytical tools to solve challenging problems in system engineering. During the 70s and 80s, numerous algorithms for the construction of state-space representations of linear systems have appeared in the controls literature. Although several techniques of minimum realization are available in the literature [15–18], formal direct application to modal parameter identification for flexible structures was not addressed until 1984. Under the interaction of structure and control disciplines, the Eigensystem Realization Algorithm [19, 20] was developed for modal parameter identification and model reduction of dynamic systems using test data. During the 90s, many system identification techniques have been developed and/or applied to identify a state-space model for modal parameter identification of large flexible aerospace structures, such as the Hubble Spacecraft Telescope [21]. The Observer/Kalman Identification (OKID) algorithm, formulated entirely in the time-domain, computes the Markov parameters of a time invariant linear system, from which the state-space model and a corresponding observer are determined simultaneously [22]. In parallel, several efforts have been made for developing time-varying models and to generalize ERA to the case of time-varying systems. Development of methods for time-varying systems have involved recursive and fast implementations of the time invariant methods by exploring structural properties of the input–output realizations [23] or by generalizing several concepts in the classical linear time invariant system theory consistently [24, 25]. Later, the idea of repeated experiments have been introduced [26, 27] and presented as practical methods to realize the conceptual state space model identification strategies presented earlier. From a perspective of generalizing the ERA to the case of time-varying systems Majji, Juang and Junkins [28] developed a time-varying version of ERA. Additionally, they showed that the generalization thus made enables the identification of time-varying plant models that are in arbitrary coordinate systems at each time step and that the coordinate systems at successive time steps are compatible with one another, making the model sequences realized useful in state propagation. In complement, using an asymptotically stable observer (to remedy the problem of unbounded growth in the number of experiments), they developed the time-varying observer/Kalman-filter system identification (TVOKID) to work with TVERA.

In 2010, Schmid [30] introduces a Dynamic Mode Decomposition (DMD) algorithm to extract dynamic information from flow fields either from simulated models or physical experiments. The extracted dynamic modes are associated to a lower dimensional subspace which best describes the underlying physical mechanisms captured in the data sequence with significantly fewer degrees of freedom. Originally introduced in the fluid mechanics community, the original authors of DMD never realized nor acknowledge that DMD is indeed a special case of ERA. A few years later, it is shown that while DMD and the ERA were developed in different contexts, they are closely related: the low-order linear operators central to each method are only related by a similarity transform [31]. Furthermore, DMD has been designed to analyze data generated by any dynamical system (the system can be nonlinear and may have inputs) but does not originally explicit how to get input-influence or output-influence matrices, which ERA does. More importantly, DMD is missing the important concept of kinematic similarity among linear discrete-time-varying system models and the time-varying transformations involved in the state transition matrices.

This paper aims to demonstrate the capabilities of these algorithm to provide a reduced-order model to reproduce the aerothermoelastic response of a hypersonic vehicle. Section II will briefly introduce the basic concepts of realization for time-varying systems while Section III will provide a detailed description of TVERA for autonomous systems and a step by step procedure to compute the state-space matrices of a reduced-order identified system from experimental data only. To validate the developed approach, Section IV considers two numerical simulations involving the nonlinear dynamics of a simplistic heated panel as well as a high-fidelity simulation that couples the aeroelastic response during atmospheric flight.

II. Problem Statement

Although almost every physical system contains nonlinearities, oftentimes its behavior within a certain operating range of a nominal trajectory can be reasonably approximated by that of a linear model. One reason for approximating

the nonlinear system by a linear model of the form is that one can apply rather simple and systematic linear control or extract quantities that are representative of the true system behavior. These parameters are related to some intrinsic characteristics of the systems and are useful to the analyst (eigenvalues and eigenvectors are related to the natural frequencies and modes of the system for example).

Start with a simple first-order nonlinear dynamic system

$$\dot{\boldsymbol{x}}(t) = \boldsymbol{f}(\boldsymbol{x}(t), \boldsymbol{u}(t)), \quad \text{with } \boldsymbol{x}(0) = \boldsymbol{x}_0, \tag{1}$$

along with a measurement equation

$$\boldsymbol{y}(t) = \boldsymbol{g}(\boldsymbol{x}(t), \boldsymbol{u}(t)). \tag{2}$$

Assume that under usual working circumstances this system operates along the trajectory $\boldsymbol{x}^\star(t)$ while it is driven by the system input $\boldsymbol{u}^\star(t)$. $\boldsymbol{x}^\star$ and $\boldsymbol{u}^\star$ are called the nominal system trajectory and the nominal system input, respectively. On the nominal trajectory the following differential equation is satisfied

$$\dot{\boldsymbol{x}}^\star(t) = \boldsymbol{f}(\boldsymbol{x}^\star(t), \boldsymbol{u}^\star(t)), \quad \text{with } \boldsymbol{x}^\star(0) = \boldsymbol{x}_0^\star, \tag{3a}$$

$$\boldsymbol{y}^\star(t) = \boldsymbol{g}(\boldsymbol{x}^\star(t), \boldsymbol{u}^\star(t)). \tag{3b}$$

Assume that the motion of the nonlinear system is in the neighborhood of the nominal system trajectory, that is

$$\boldsymbol{x}(t) = \boldsymbol{x}^\star(t) + \delta\boldsymbol{x}(t), \tag{4}$$

sustained by a system input close to the nominal input

$$\boldsymbol{u}(t) = \boldsymbol{u}^\star(t) + \delta\boldsymbol{u}(t). \tag{5}$$

The departure dynamics is the dynamical system verified by $\delta\boldsymbol{x}(t)$ and $\delta\boldsymbol{u}(t)$, that is

$$\delta\dot{\boldsymbol{x}}(t) = A_c(t)\delta\boldsymbol{x}(t) + B_c(t)\delta\boldsymbol{u}(t), \quad \text{with } \delta\boldsymbol{x}(0) = \delta\boldsymbol{x}_0, \tag{6a}$$

$$\delta\boldsymbol{y}(t) = C(t)\delta\boldsymbol{x}(t) + D(t)\delta\boldsymbol{u}(t), \tag{6b}$$

with

$$A_c(t) = \left.\frac{\partial \boldsymbol{f}}{\partial \boldsymbol{x}}\right|_{\boldsymbol{x}^\star(t),\boldsymbol{u}^\star(t)}, \tag{7a}$$

$$B_c(t) = \left.\frac{\partial \boldsymbol{f}}{\partial \boldsymbol{u}}\right|_{\boldsymbol{x}^\star(t),\boldsymbol{u}^\star(t)}, \tag{7b}$$

$$C(t) = \left.\frac{\partial \boldsymbol{g}}{\partial \boldsymbol{x}}\right|_{\boldsymbol{x}^\star(t),\boldsymbol{u}^\star(t)}, \tag{7c}$$

$$D(t) = \left.\frac{\partial \boldsymbol{g}}{\partial \boldsymbol{u}}\right|_{\boldsymbol{x}^\star(t),\boldsymbol{u}^\star(t)}. \tag{7d}$$

In discrete-time, these equations become

$$\delta\boldsymbol{x}(k+1) = A_k\delta\boldsymbol{x}(k) + B_k\delta\boldsymbol{u}(k) \tag{8a}$$

$$\delta\boldsymbol{y}(k) = C_k\delta\boldsymbol{x}(k) + D_k\delta\boldsymbol{u}(k) \tag{8b}$$

The time-varying system identification algorithm developed in this paper will be used to compute a realization of the system matrices $\{A_k, B_k, C_k, D_k\}$.

III. General Methodology

A. Preliminaries on time-varying System Identification

Due to its efficiency and robustness of implementation in numerous areas of engineering, the Eigensystem Realization Algorithm (ERA) has occupied a central stage in the current and expansive field of system identification. As a consequence, the associated algorithms have contributed to several successful applications in design, control, and model order reduction of dynamical systems.

The most crucial advancement in the realization theory of time-varying systems thus far is the effects of time-varying coordinate systems. In contrast with time invariant (shift invariant) systems, state matrices of two different realizations of a time-varying system are not similar. From an input and output standpoint, two realizations of the same system are said to be topologically equivalent and the state matrices sequence said to be kinematically similar. Figure 1 highlights the main difference between equivalence and topological equivalence for time-invariant and time-varying systems.

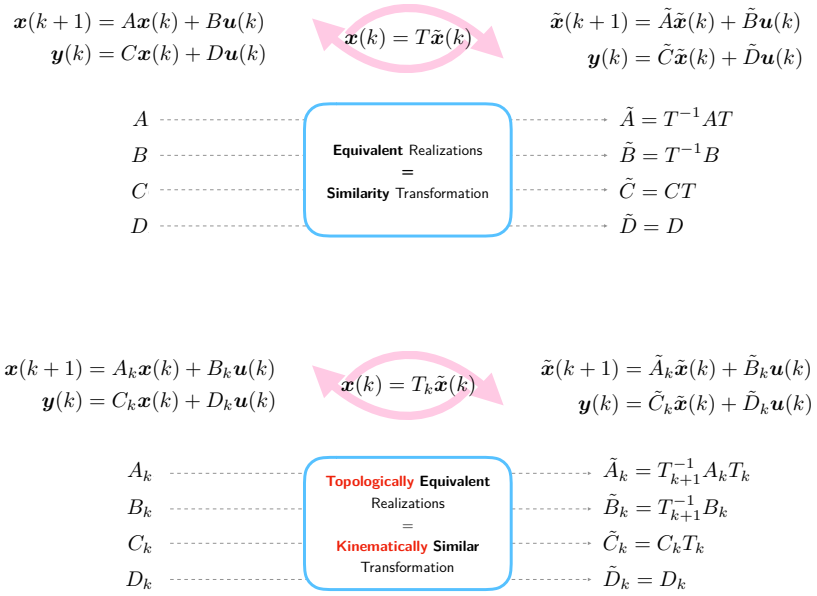

Fig. 1 Linear time-invariant and linear time-varying systems: difference between equivalence and topological equivalence

In general, the identified system representation $\{\hat{A}_k, \hat{B}_k, \hat{C}_k, \hat{D}_k\}$ at each time k is not represented in the same coordinate system as the true system representation $\{A_k, B_k, C_k, D_k\}$ and the state propagation for linear time-varying systems takes place between time-varying coordinate systems. While the system matrices do not need any type of correction during the propagation itself (we will see that these matrices come from the same SVD at each time step), two equivalent realizations $\{A_k, B_k, C_k, D_k\}$ and $\{\hat{A}_k, \hat{B}_k\ \hat{C}_k\ \hat{B}_k\}$ are not similar; rather they are topologically equivalent. Topological equivalence (or kinematic equivalence) means that there exists a sequence of invertible, square matrices (not necessarily related to each other, Lyapunov transformations) T_k such that

$$\hat{A}_k = T_{k+1}^{-1}A_kT_k \tag{9}$$

$$\hat{B}_k = T_{k+1}^{-1}B_k \tag{10}$$

$$\hat{C}_k = C_kT_k \tag{11}$$

$$\hat{D}_k = D_k \tag{12}$$

The most important diagnosis to make is that the identified system matrix $\hat{A}_k$ and the true system matrix A_k do not have the same eigenvalues. Because the system evolution takes place in two different coordinate systems, T_{k+1} and T_k, this leads the basis vectors for the initial time step and the final time step to be different. Therefore, the situation is quite similar to body-fixed, rotating coordinate systems in rigid body dynamics, with the exception that the frames

(basis vectors can be thought of as frames) are unknown, arbitrarily assigned by the singular value decomposition. However, one can extract time-varying quantities that are representative of the true time-varying system behavior from these topologically equivalent (kinematically similar) transformations. These parameters are the eigenvalues of the time-varying system matrices (true and identified) all transformed into a reference coordinate system. In order to do so, define the quantity

$$\hat{\boldsymbol{O}}_k^{(p)^\dagger}\hat{\boldsymbol{O}}_{k+1}^{(p)} = T_k^{-1}\boldsymbol{O}_k^{(p)^\dagger}\boldsymbol{O}_{k+1}^{(p)}T_{k+1}, \tag{13}$$

with $\boldsymbol{O}_k^{(p)}$ is the observability matrix at time k

$$\boldsymbol{O}_k^{(p)} = \begin{bmatrix} C_k \\ C_{k+1}A_k \\ C_{k+2}A_{k+1}A_k \\ \vdots \\ C_{k+p-1}A_{k+p-2}\dots A_k \end{bmatrix}, \tag{14}$$

Now we proceed to use the correction to the left of $\hat{A}_k$ and obtain a corrected system matrix

$$\tilde{\hat{A}}_k = \hat{\boldsymbol{O}}_k^{(p)^\dagger}\hat{\boldsymbol{O}}_{k+1}^{(p)}\hat{A}_k = T_k^{-1}\boldsymbol{O}_k^{(p)^\dagger}\boldsymbol{O}_{k+1}^{(p)}T_{k+1}T_{k+1}^{-1}A_kT_k = T_k^{-1}\boldsymbol{O}_k^{(p)^\dagger}\boldsymbol{O}_{k+1}^{(p)}A_kT_k = T_k^{-1}\tilde{A}_kT_k, \tag{15}$$

and the matrices $\tilde{\hat{A}}_k$ and $\tilde{A}_k$ are now equivalent. This is a central result for the time-varying eigensystem realization algorithm. For the system identification problem, when the true and identified systems are kinematically similar realizations, the identified and true system share common eigenvalues after transformation.

B. Time-varying Eigensystem Realization Algorithm for an autonomous system (TVERA)

This section introduces the basics of time-varying linear system identification for time-varying linear systems subject to an initial condition response (autonomous system). A linear discrete-time varying autonomous system is given by

$$\boldsymbol{x}(k+1) = A_k\boldsymbol{x}(k) \tag{16a}$$
$$\boldsymbol{y}(k) = C_k\boldsymbol{x}(k) \tag{16b}$$

together with an initial state vector $\boldsymbol{x}(0)$, where $\boldsymbol{x}(k) \in \mathbb{R}^n$ and $\boldsymbol{y}(k) \in \mathbb{R}^m$ are the state and output vectors respectively, $k \geq 0$. The time-varying (non constant) matrices A_k and C_k with appropriate dimensions represent the internal operation of the linear system, and are used to determine the system's response to any arbitrary initial condition. The solution of the difference equation, given in Eqs. (16) is given by

$$\boldsymbol{x}(k) = \Phi(k,0)\boldsymbol{x}(0), \tag{17a}$$
$$\boldsymbol{y}(k) = C_k\Phi(k,0)\boldsymbol{x}(0), \tag{17b}$$

where the state transition matrix is defined in terms of its components by

$$\Phi(k,k_0) = \begin{cases} A_{k-1}A_{k-2}\dots A_{k_0} & \text{for } k > k_0, \\ I & \text{for } k = k_0, \\ \text{undefined} & \text{for } k < k_0. \end{cases} \tag{18}$$

The method for computing the system matrices using a set of experimental data $\{\boldsymbol{y}^{\#i}\}_{i=1..N}$ (free response experiments) involves the construction of the matrix $\tilde{\boldsymbol{H}}_k^{(p,N)}$,

$$\tilde{\boldsymbol{H}}_k^{(p,N)} = \begin{bmatrix} \boldsymbol{y}_k^{\#1} & \boldsymbol{y}_k^{\#2} & \cdots & \boldsymbol{y}_k^{\#N} \\ \boldsymbol{y}_{k+1}^{\#1} & \boldsymbol{y}_{k+1}^{\#2} & \cdots & \boldsymbol{y}_{k+1}^{\#N} \\ \vdots & \vdots & \ddots & \vdots \\ \boldsymbol{y}_{k+p-1}^{\#1} & \boldsymbol{y}_{k+p-1}^{\#2} & \cdots & \boldsymbol{y}_{k+p-1}^{\#N} \end{bmatrix} = \boldsymbol{O}_k^{(p)}\boldsymbol{X}_k^{(N)}, \tag{19}$$

where $\boldsymbol{O}_k^{(p)}$ is the observability matrix at time k

$$\boldsymbol{O}_k^{(p)} = \begin{bmatrix} C_k \\ C_{k+1}A_k \\ C_{k+2}A_{k+1}A_k \\ \vdots \\ C_{k+p-1}A_{k+p-2}\dots A_k \end{bmatrix}, \tag{20}$$

and $\boldsymbol{X}_k^{(N)}$ is a state variable ensemble at time k:

$$\boldsymbol{X}_k^{(N)} = \begin{bmatrix} \Phi(k,0)\boldsymbol{x}_0^{\#1} & \Phi(k,0)\boldsymbol{x}_0^{\#2} & \cdots & \Phi(k,0)\boldsymbol{x}_0^{\#N} \end{bmatrix} \in \mathbb{R}^{n\times N}. \tag{21}$$

The state variables $\boldsymbol{x}_0^{\#1}, \boldsymbol{x}_0^{\#2}, \dots, \boldsymbol{x}_0^{\#N}$ are simply the initial conditions from where the free response experiments are derived. The parameter p and the number of free response experiments N are chosen such that the matrix $\tilde{\boldsymbol{H}}_k^{(p,N)}$ retains the rank n, the true state dimension. Indeed, if $pm \geq n$ and $N \geq n$, matrices $\boldsymbol{O}_k^{(p)}$ and $\boldsymbol{X}_k^{(N)}$ are of rank maximum n (equal to n for $\boldsymbol{X}_k^{(N)}$). If the system is observable, the block matrix $\boldsymbol{O}_k^{(p)}$ is of rank exactly n and so is $\tilde{\boldsymbol{H}}_k^{(p,N)}$. Identifying the number of dominant singular values of the Hankel matrix will thus provide an indication about the unknown order of the reduced model to be identified. Differing ranks are possible for this generalized time-varying matrix $\tilde{\boldsymbol{H}}_k^{(p,N)}$ at every time step for the variable state dimension problem. However, it is assumed that the state dimension does not change with the time index and it is not difficult to see that this assumption can be relaxed, given some adjustments. We retain the assumption owing to our focus on mechanical systems, in which the connection between physical degrees of freedom and the number of state variables allows us to hold the dimensionality of the state space fixed throughout the time interval of interest.

As for the general procedure in ERA or TVERA, using the singular value decomposition of $\tilde{\boldsymbol{H}}_k^{(p,N)}$, we can write

$$\tilde{\boldsymbol{H}}_k^{(p,N)} = \boldsymbol{U}_k\boldsymbol{\Sigma}_k\boldsymbol{V}_k^{\intercal} = \begin{bmatrix} \boldsymbol{U}_k^{(n)} & \boldsymbol{U}_k^{(0)} \end{bmatrix} \begin{bmatrix} \boldsymbol{\Sigma}_k^{(n)} & \boldsymbol{0} \\ \boldsymbol{0} & \boldsymbol{\Sigma}_k^{(0)} \end{bmatrix} \begin{bmatrix} \boldsymbol{V}_k^{(n)\intercal} \\ \boldsymbol{V}_k^{(0)\intercal} \end{bmatrix} \tag{22a}$$

$$= \boldsymbol{U}_k^{(n)}\boldsymbol{\Sigma}_k^{(n)}\boldsymbol{V}_k^{(n)\intercal} + \underbrace{\boldsymbol{U}_k^{(0)}\boldsymbol{\Sigma}_k^{(0)}\boldsymbol{V}_k^{(0)\intercal}}_{\simeq\boldsymbol{0}} \tag{22b}$$

$$\simeq \boldsymbol{U}_k^{(n)}\boldsymbol{\Sigma}_k^{(n)}\boldsymbol{V}_k^{(n)\intercal} \tag{22c}$$

where the approximation at a given time step k is made possible by rejecting the small singular values. Indeed, some singular values of $\boldsymbol{\Sigma}_k$ may be relatively small and negligible in the sense that they contain more noise information than system information. Hence, the approximation $\boldsymbol{U}_k^{(0)}\boldsymbol{\Sigma}_k^{(0)}\boldsymbol{V}^{(0)\intercal}_k \simeq \boldsymbol{0}$ (truncation of nonzero small singular values) is to account for noise in the data and for quantitatively partitioning the realized model into principal and perturbation (noise) portions so that the noise portion can be disregarded. In other words, the directions determined by these singular values have less significant degrees of observability relative to noise. The reduced model of order n after deleting these singular values is then considered as the robustly observable part of the realized system. In terms of the corresponding observability and state variable ensemble matrices,

$$\tilde{\boldsymbol{H}}_k^{(p,N)} = \boldsymbol{U}_k^{(n)}\boldsymbol{\Sigma}_k^{(n)}\boldsymbol{V}_k^{(n)\intercal} = \boldsymbol{O}_k^{(p)}\boldsymbol{X}_k^{(N)} \Rightarrow \begin{cases} \boldsymbol{O}_k^{(p)} = \boldsymbol{U}_k^{(n)}\boldsymbol{\Sigma}_k^{(n)\,1/2} \\ \boldsymbol{X}_k^{(N)} = \boldsymbol{\Sigma}_k^{(n)\,1/2}\boldsymbol{V}_k^{(n)\intercal} \end{cases}. \tag{23}$$

The same procedure at time step $k+1$ will lead to

$$\tilde{\boldsymbol{H}}_{k+1}^{(p,N)} = \boldsymbol{U}_{k+1}^{(n)}\boldsymbol{\Sigma}_{k+1}^{(n)}\boldsymbol{V}_{k+1}^{(n)\;\intercal} = \boldsymbol{O}_{k+1}^{(p)}\boldsymbol{X}_{k+1}^{(N)} \Rightarrow \begin{cases} \boldsymbol{O}_{k+1}^{(p)} = \boldsymbol{U}_{k+1}^{(n)}\boldsymbol{\Sigma}_{k+1}^{(n)\;1/2} \\ \boldsymbol{X}_{k+1}^{(N)} = \boldsymbol{\Sigma}_{k+1}^{(n)\;1/2}\boldsymbol{V}_{k+1}^{(n)\;\intercal} \end{cases}. \tag{24}$$

Note that the state variable ensemble matrix $\boldsymbol{X}_{k+1}^{(N)}$ at time $k+1$ is related to the state variable ensemble matrix $\boldsymbol{X}_k^{(N)}$ at time k by

$$\boldsymbol{X}_{k+1}^{(N)} = A_k\boldsymbol{X}_k^{(N)} \tag{25}$$

which leads to the estimate

$$\hat{A}_k = \boldsymbol{X}_{k+1}^{(N)} \boldsymbol{X}_k^{(N)^{-1}} \tag{26}$$

for the time-varying state matrix. The calculation of the corresponding $\hat{C}_k$ is accomplished by setting

$$\hat{C}_k = \boldsymbol{O}_k^{(p)}[0:m,:]. \tag{27}$$

Finally, in case the initial condition of the signal of interest is not part of the state variable ensemble at time 0, $\boldsymbol{X}_0^{(N)}$, one needs to identify the initial condition with an additional development. Writing the general expression of the output at the initial time for an additional p more time steps, one obtain a set of equations that can be written in a matrix form as

$$\boldsymbol{y}^{(p)}(0) = \boldsymbol{O}_0^{(p)} \boldsymbol{x}(0) \tag{28}$$

with

$$\boldsymbol{y}^{(p)}(0) = \begin{bmatrix} \boldsymbol{y}(0) \\ \boldsymbol{y}(1) \\ \vdots \\ \boldsymbol{y}(p-1) \end{bmatrix}, \quad \boldsymbol{O}_0^{(p)} = \begin{bmatrix} C_0 \\ C_1 A_0 \\ C_2 A_1 A_0 \\ \vdots \\ C_{p-1} A_{p-2} \dots A_0 \end{bmatrix}. \tag{29}$$

Eq. (28) can be solved using the least-squares solution:

$$\hat{\boldsymbol{x}}(0) = \boldsymbol{O}_0^{(p)^\dagger} \boldsymbol{y}^{(p)}(0). \tag{30}$$

IV. Numerical simulations

This section aims to demonstrate the efficacy of the proposed approach for identifying a reduced-order model of a coupled thermal-structural response in an aerothermoelastic simulation. Two cases are considered. First, a simplistic model for the flutter of a panel with prescribed increasing temperature is studied. This numerical simulation allows us to demonstrate the capability of the developed algorithm on a low order model where the measurements are of low dimension. Second, a fully-coupled nonlinear aerothermoelastic models is studied. This numerical simulation demonstrates the generalizability of the TVERA algorithm to high-dimensional problems.

A. The panel flutter problem

The supposed unknown nondimensionalized equations for the flutter of a panel are [14]

$$\frac{1}{2}\pi^4 q_1(t) - 5\pi^2 R_T q_1(t) + \frac{5}{4}\pi^4 q_1^3(t) - \frac{4}{3}\lambda q_2(t) + 5\pi^4 q_1(t) q_2^2(t) + \frac{1}{2}\sqrt{\frac{\lambda\mu}{M}} q_1'(t) + \frac{1}{2} q_1''(t) = 0, \tag{31a}$$

$$\frac{4}{3}\lambda q_1(t) + 8\pi^4 q_2(t) - 20\pi^2 R_T q_2(t) + 5\pi^4 q_1^2(t) q_2(t) + 20\pi^4 q_2^3(t) + \frac{1}{2}\sqrt{\frac{\lambda\mu}{M}} q_2'(t) + \frac{1}{2} q_2''(t) = 0. \tag{31b}$$

where q_1 and q_2 are structural modal coordinates, λ is the dynamic pressure quantifying the aerodynamic loading, μ is the mass ratio quantifying the aerodynamic damping effect, R_T is the in-plane force due to the thermal stress. In general, when $R_T = 0$, there is a critical value λ_{cr}, such that the panel stays stable when $\lambda < \lambda_{cr}$, but enters limit cycle oscillation when $\lambda > \lambda_{cr}$. When $R_T > 0$, the critical value λ_{cr} still exists. However, the panel may become statically buckled or enter chaotic response instead of being stable, when $\lambda < \lambda_{cr}$. In this example, it is assumed that $R_T = 2t + 0.01$, i.e. the in-plane force increases linearly in time.

Let $\boldsymbol{q}(t) = \begin{bmatrix} q_1(t) & q_2(t) & q_1'(t) & q_2'(t) \end{bmatrix}^\intercal$. We introduce the function $\boldsymbol{f}$ that describes the dynamics presented above and write the dynamical system as

$$\boldsymbol{q}'(t) = \boldsymbol{f}(\boldsymbol{q}(t), t). \tag{32}$$

The linearized version of (32) is

$$\boldsymbol{q}'(t) = A_c(t)\boldsymbol{q}(t) \tag{33}$$

with

$$A_c(t) = \left.\frac{\partial \boldsymbol{f}}{\partial \boldsymbol{q}}\right|_{\boldsymbol{q}=\overline{\boldsymbol{q}}(t)} = \begin{bmatrix} 0 & 0 & 1 & 0 \\ 0 & 0 & 0 & 1 \\ -\pi^4 + 10\pi^2 R_T - \frac{15}{2}\pi^4\overline{q}_1^2(t) - 10\pi^4\overline{q}_2^2(t) & \frac{8}{3}\lambda - 20\pi^4\overline{q}_1(t)\overline{q}_2(t) & -\sqrt{\frac{\lambda\mu}{M}} & 0 \\ -\frac{8}{3}\lambda - 20\pi^4\overline{q}_1(t)\overline{q}_2(t) & -16\pi^4 + 40\pi^2 R_T - 10\pi^4\overline{q}_1^2(t) - 120\pi^4\overline{q}_2^2(t) & 0 & -\sqrt{\frac{\lambda\mu}{M}} \end{bmatrix} \tag{34}$$

where $A_c(t)$ is the continuous-time linearized version matrix of $\boldsymbol{f}$ and $\overline{\boldsymbol{q}}(t)$ is a nominal trajectory. This nominal trajectory is an initial condition response with initial state

$$\overline{\boldsymbol{q}}(0) = \begin{bmatrix} 0 & 0.001 & 0 & 0 \end{bmatrix}^\intercal, \tag{35}$$

and is referred as the *true* trajectory. Additionally, we define the measurement equations

$$\boldsymbol{y}(t) = C\boldsymbol{q}(t) \tag{36}$$

where $C = I_{4\times4}$. (33) and (36) form the first order continuous state-space dynamics. In order to compare with the identified models, analytical discrete-time models are generated by computing the state transition matrix. Indeed, integrating the state transition matrix between two consecutive time steps is the equivalent of the matrix multiplication by A_k. Because the system matrices are time varying, the matrix differential equation is given by

$$\dot{\Phi}(t, t_k) = A_c(t)\Phi(t, t_k), \quad \forall\, t \in [t_k, t_{k+1}], \tag{37}$$

with initial condition

$$\Phi(t_k, t_k) = I_{4\times4}, \tag{38}$$

such that

$$A_k = \Phi(t_{k+1}, t_k) \tag{39}$$

would represent the equivalent discrete-time varying system matrix (true model). The resulting trajectory satisfies the difference equation:

$$\boldsymbol{q}(k+1) = A_k\boldsymbol{q}(k) \tag{40a}$$

$$\boldsymbol{y}(k) = C\boldsymbol{q}(k) \tag{40b}$$

and are the analogous of (16a) and (16b) from the previous section. Note that $\boldsymbol{y}(k) = \boldsymbol{q}(k)$ since C is the identity.

The procedure to compute the identified system matrices $\hat{A}_k$ and $\hat{C}_k$ is as follow:

1) Generate N initial condition responses using (31a) and (31b) in order to form $\tilde{\boldsymbol{H}}_k^{(p,N)}$. Note that for this particular system of order $n = 4$, N and p must satisfy $N > 4$ and $pm > 4$ with $m = 4$.
2) At each time step, perform a SVD on $\tilde{\boldsymbol{H}}_k^{(p,N)}$ and find $\boldsymbol{O}_k^{(p)}$ and $\boldsymbol{X}_k^{(N)}$.
3) Compute $\hat{A}_k$ and $\hat{C}_k$ with (26) and (27).
4) Identify the initial condition of the nominal trajectory using the previous developments from (28) to (30).

The system matrices thus obtained are used to propagate the trajectory. For this simulation, four random initial conditions are considered (with a standard deviation of 10^{-3} around the nominal), resulting in $N = 4$. p is chosen to be 1 and the data is recorded at a frequency of 50Hz for 5 sec. Figure 2 shows how the identified system performs compared to the local linearization approximated trajectory. The TVERA procedure is able to provide a linear time-varying system that approximates the dynamics of the nonlinear system presented above. Absolute and RMS errors are presented in

Table 1. While both identified and linearized systems seems to be a good linear approximation for the true system, the linearized version completely degrades once it enters the oscillatory regime. On the other hand, the identified system is able to capture the long-term trend over the time interval of interest. Figure 3 shows the evolution of the SVD decomposition of the matrix $\tilde{\boldsymbol{H}}_k^{(p,N)}$. One can observe four dominant singular values at each time step, consistent with the actual order $n = 4$ of the system.

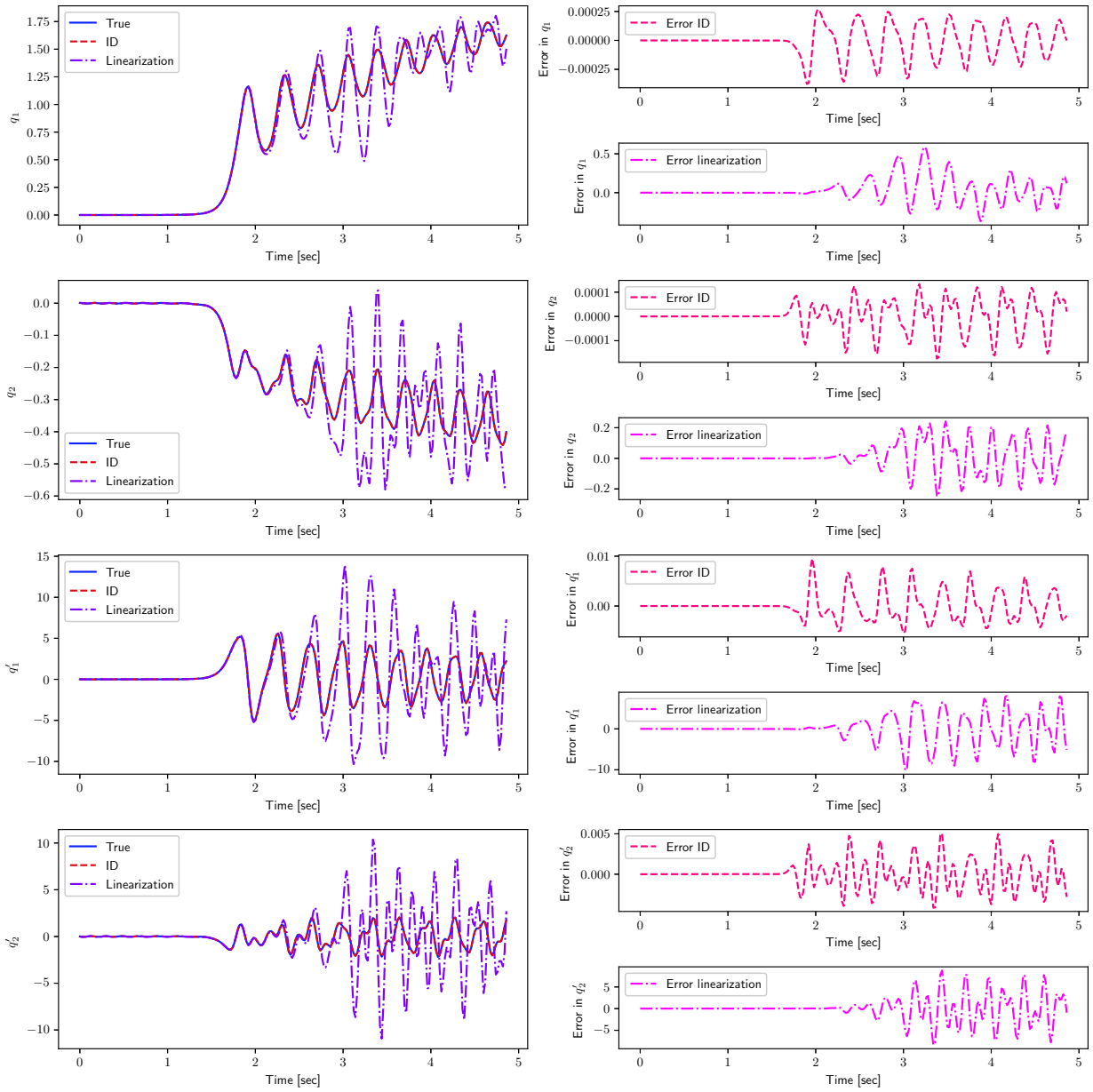

Fig. 2 Error in propagation for the identified model and the actual true linearization

Table 1 Identification Errors

Output	RMS Error		Mean Absolute Error	
	Identified System	Linearized System	Identified System	Linearized System
q_1	$3.74 \cdot 10^{-3}$	$3.57 \cdot 10^{-1}$	$2.63 \cdot 10^{-3}$	$2.12 \cdot 10^{-1}$
q_2	$1.69 \cdot 10^{-3}$	$2.14 \cdot 10^{-1}$	$1.14 \cdot 10^{-3}$	$1.33 \cdot 10^{-1}$
q_1'	$7.75 \cdot 10^{-2}$	7.83	$5.12 \cdot 10^{-2}$	4.85
q_2'	$4.79 \cdot 10^{-2}$	6.73	$3.16 \cdot 10^{-2}$	3.89

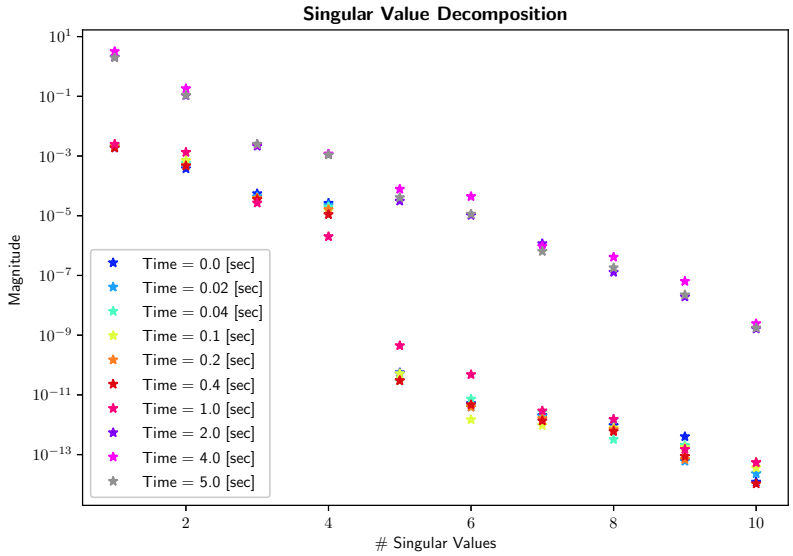

Fig. 3 Evolution of the magnitude of the singular values from singular value decomposition

The TVERA approximation turns out to be more accurate than the local linearization thanks to the singular value decomposition at the heart of the procedure. Since the Moore-Penrose pseudoinverse (or peudoinverse in short) is a natural consequence from applying the singular value decomposition to the least squares problem, the SVD resolves the least squares problem into two components: (1) a range space part which can be minimized, and (2) a null space term which cannot be removed - a residual error, due to the fact that the system is over-constrained. Hence, while TVERA provides a least-square solution for A_k at each time step over a time interval, the linearized (or true) A_k represents the local tangent at time t_k. The linearization does not benefit from values in the neighborhood of t_k to compute the best linear approximation at time t_k, which TVERA takes advantage of.

B. High-dimensional nonlinear aerothermoelastic simulation

Subsequently, the same type of analysis is applied to a high-dimensional nonlinear aerothermoelastic problem. The aerothermoelastic simulation is performed using the HYPATE framework, which has been extensively verified and applied to various hypersonic aerothermoelastic problems [3, 12]. In this study, the low-fidelity portion of the framework is employed. In the aerothermodynamic solver, the pressure and the heat flux are computed using full-order piston theory and Eckert's reference enthalpy method, respectively. The structural and thermal solvers are both based on the finite element formulation. The structural solver models the structural dynamics of anisotropic (i.e. composite) shallow shells with shear, geometric nonlinearity, and thermal stress. The thermal solver models heat transfer in composite shells using a layer-wise thermal lamination theory. Both solvers account for temperature-dependent material properties. The solvers of the three physical domains are solved using a second-order time-accurate loosely-coupled scheme.

In this example, a 2D skin panel configuration is considered, as shown in Figure 4. The panel is simply supported at the leading and trailing edges. The geometrical parameters are $h = 5$mm, $a = 1$m, and $L_{le} = 1$m. The panel is made of

Al7075 and the material properties are temperature dependent. The initial temperature is $T = 273K$.

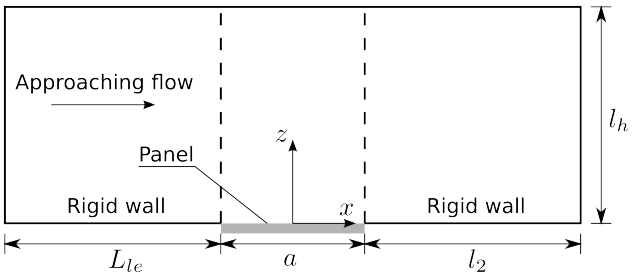

Fig. 4 2D skin panel configuration

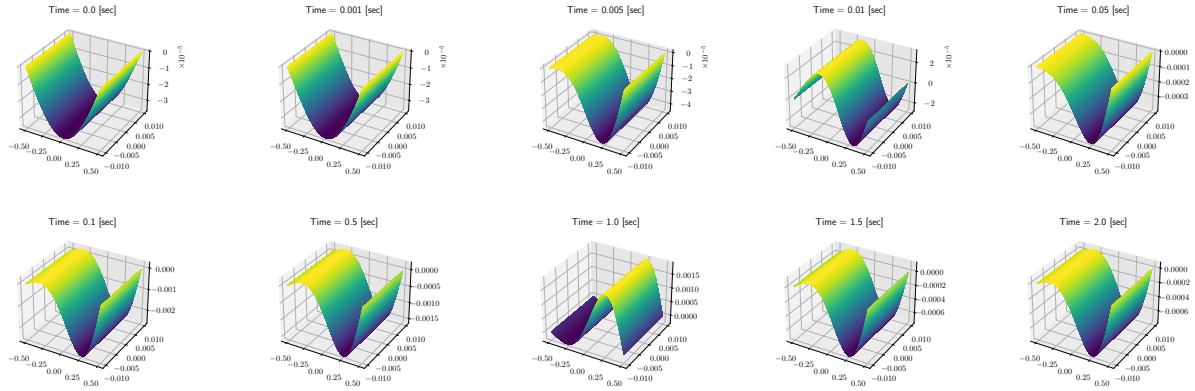

Fig. 5 Evolution of the panel shape over the time

The measurement equation is now directly about the displacement of the structure, creating a vector of dimension 101. The initial absolute perturbation applied to the panel ranges from $8 \cdot 10^{-5}$ Pa to $1 \cdot 10^{-4}$ Pa. Two sets of experiment are created for the study: one will serve as a training set for TVERA and one will be used for testing the accuracy of the derived model. The specifics for each set re gathered in Table 1. The numerical data is acquired for 2 seconds at a frequency of 1000 Hz resulting in 2001 data points. The procedure we employ for this numerical simulation is similar as before and a reduced model of order $n = 6$ has been found to be the most accurate. Although the resulting order of the reduced model is usually found by examining the singular value decomposition plot, the one provided Figure 6 doesn't allow the analyst to gain too much insight. While it seems that 6 singular values could be found to be of greater magnitude than the rest of the sequence, it is difficult to acknowledge the presence of a clear cut criteria, especially as time increases.

Figures 7 and 8 show the evolution of the modes shape throughout the time for the true and the identified systems. The Figures present a sample of six responses from the training and testing sets. The identified linear time-varying model is able to capture the deformation of the panel correctly, with more accuracy for lower times. As time increases, the identified model tends to over estimates the magnitude of the deformation although capturing the right modes. An other visualization is presented with Figures 9 and 10 displaying the mid-point displacement of the panel. The left columns superimpose the true and the identified models while the right columns disclose the error between the two. Tables 3 and 4 gather the relevant identification errors for the training and testing data sets. While the peak to peak amplitudes, frequencies and phases errors are minor, the shift in magnitude is the main source of error.

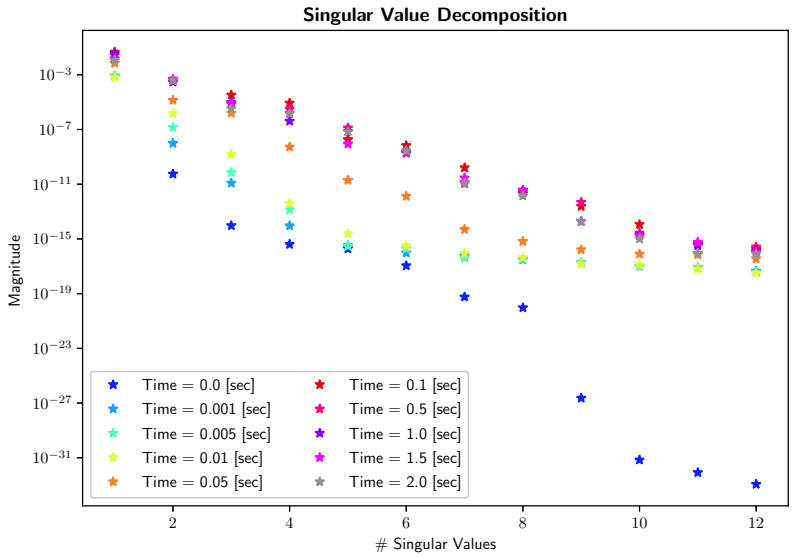

Fig. 6 Evolution of the magnitude of the singularvalues from singularvalue decomposition

Table 2 Values of the initial perturbation for both sets of experiments

Training Set	Testing Set
$-1.0 \cdot 10^{-4}$ Pa	$-9.8 \cdot 10^{-5}$ Pa
$-9.6 \cdot 10^{-5}$ Pa	$-9.5 \cdot 10^{-5}$ Pa
$-9.2 \cdot 10^{-5}$ Pa	$-9.4 \cdot 10^{-5}$ Pa
$-8.8 \cdot 10^{-5}$ Pa	$-9.0 \cdot 10^{-5}$ Pa
$-8.4 \cdot 10^{-5}$ Pa	$-8.6 \cdot 10^{-5}$ Pa
$-8.0 \cdot 10^{-5}$ Pa	$-8.5 \cdot 10^{-5}$ Pa
$+8.0 \cdot 10^{-5}$ Pa	$-8.2 \cdot 10^{-5}$ Pa
$+8.4 \cdot 10^{-5}$ Pa	$+8.2 \cdot 10^{-5}$ Pa
$+8.8 \cdot 10^{-5}$ Pa	$+8.5 \cdot 10^{-5}$ Pa
$+9.2 \cdot 10^{-5}$ Pa	$+8.6 \cdot 10^{-5}$ Pa
$+9.6 \cdot 10^{-5}$ Pa	$+9.0 \cdot 10^{-5}$ Pa
$+1.0 \cdot 10^{-4}$ Pa	$+9.4 \cdot 10^{-5}$ Pa
	$+9.5 \cdot 10^{-5}$ Pa
	$+9.8 \cdot 10^{-5}$ Pa

Table 3 Identification Errors for the Training Set

True Signal	**Training Set**			
Peak to peak Amp.	Worst error	Best error	RMSE	Average abs error
$6.8519 \cdot 10^{-4}$	$4.87 \cdot 10^{-6}$	$2.01 \cdot 10^{-7}$	$2.03 \cdot 10^{-6}$	$3.15 \cdot 10^{-6}$
Frequency	Worst error	Best error	RMSE	Average abs error
45.098	$1.26 \cdot 10^{-7}$	$2.25 \cdot 10^{-9}$	$1.44 \cdot 10^{-8}$	$5.69 \cdot 10^{-8}$
Phase	Worst error	Best error	RMSE	Average abs error
0	$6.57 \cdot 10^{-3}$	$2.66 \cdot 10^{-6}$	$5.31 \cdot 10^{-4}$	$1.01 \cdot 10^{-3}$
Shift	Worst error	Best error	RMSE	Average abs error
0	$9.95 \cdot 10^{-6}$	$6.30 \cdot 10^{-8}$	$8.76 \cdot 10^{-7}$	$9.65 \cdot 10^{-7}$

Table 4 Identification Errors for the Testing Set

True Signal	**Testing Set**			
Peak to peak Amp.	Worst	Best	RMSE	Average abs error
$6.8519 \cdot 10^{-4}$	$4.12 \cdot 10^{-6}$	$2.23 \cdot 10^{-6}$	$2.56 \cdot 10^{-6}$	$3.89 \cdot 10^{-6}$
Frequency	Worst	Best	RMSE	Average abs error
45.098	$2.99 \cdot 10^{-7}$	$6.37 \cdot 10^{-9}$	$2.30 \cdot 10^{-8}$	$8.51 \cdot 10^{-8}$
Phase	Worst	Best	RMSE	Average abs error
0	$9.85 \cdot 10^{-3}$	$4.49 \cdot 10^{-6}$	$4.21 \cdot 10^{-4}$	$8.41 \cdot 10^{-4}$
Shift	Worst	Best	RMSE	Average abs error
0	$1.20 \cdot 10^{-5}$	$5.10 \cdot 10^{-7}$	$9.91 \cdot 10^{-7}$	$1.03 \cdot 10^{-6}$

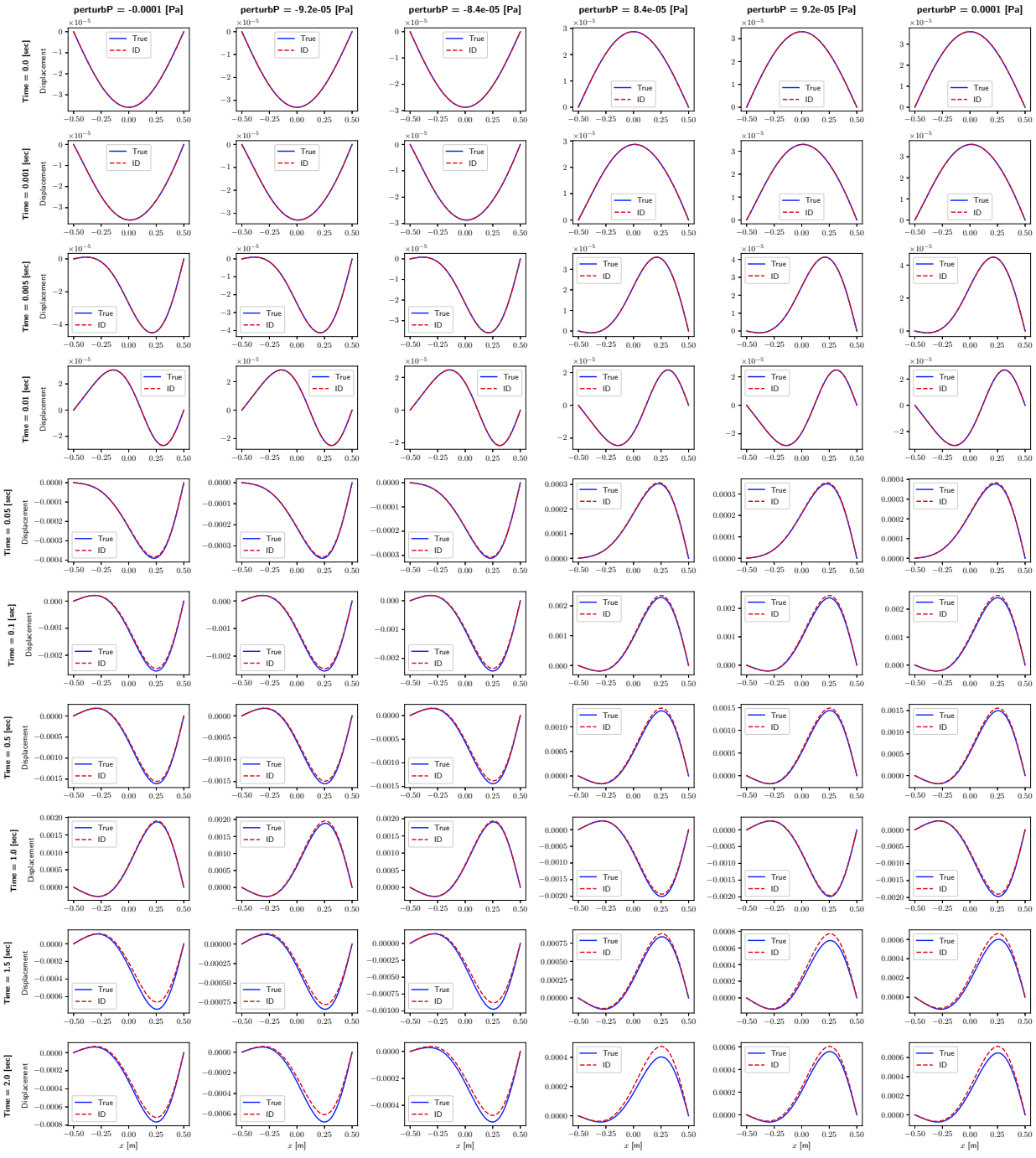

Fig. 7 Illustration of the modes shape for six responses from the training set

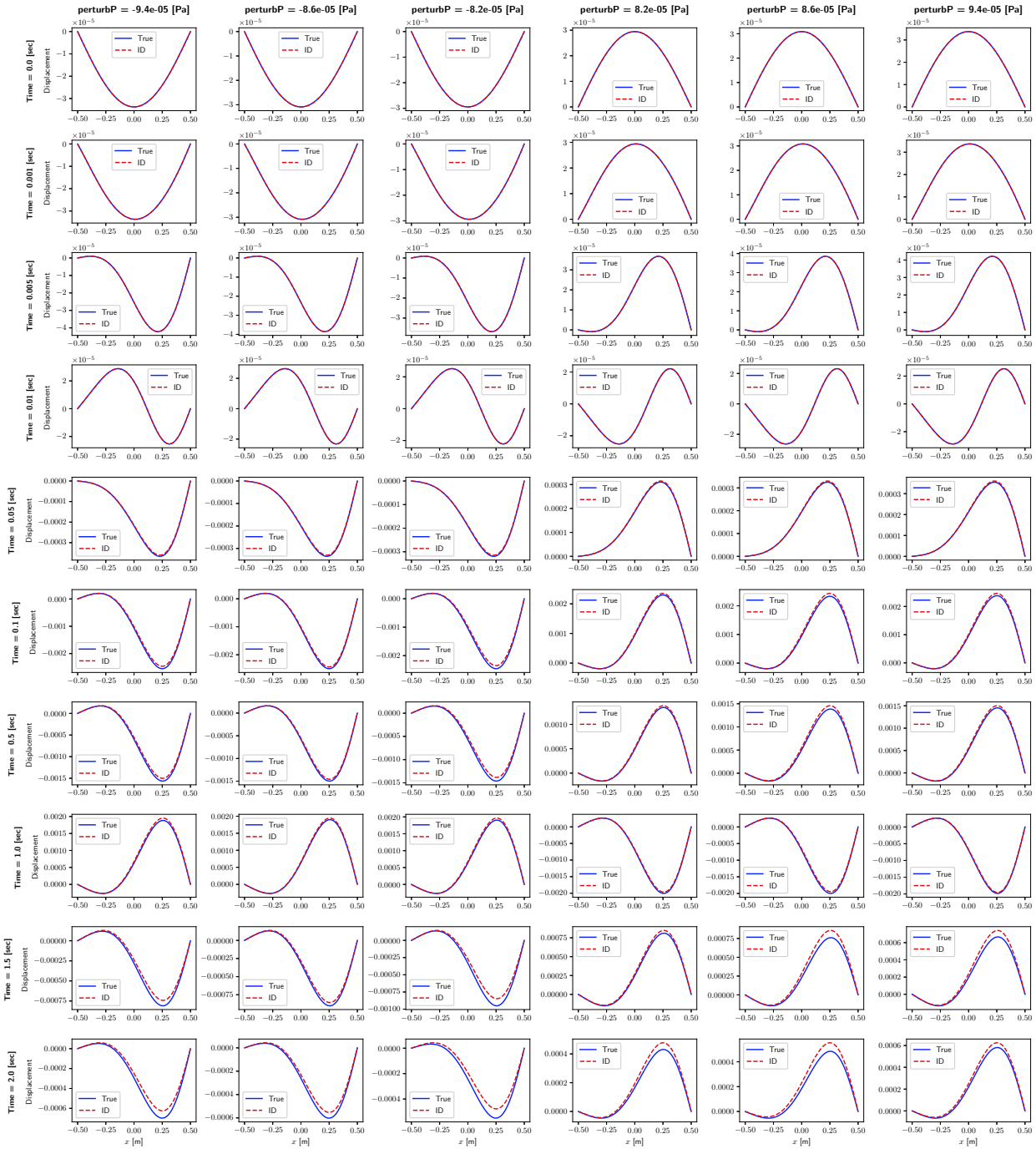

Fig. 8 Illustration of the modes shape for six responses from the testing set

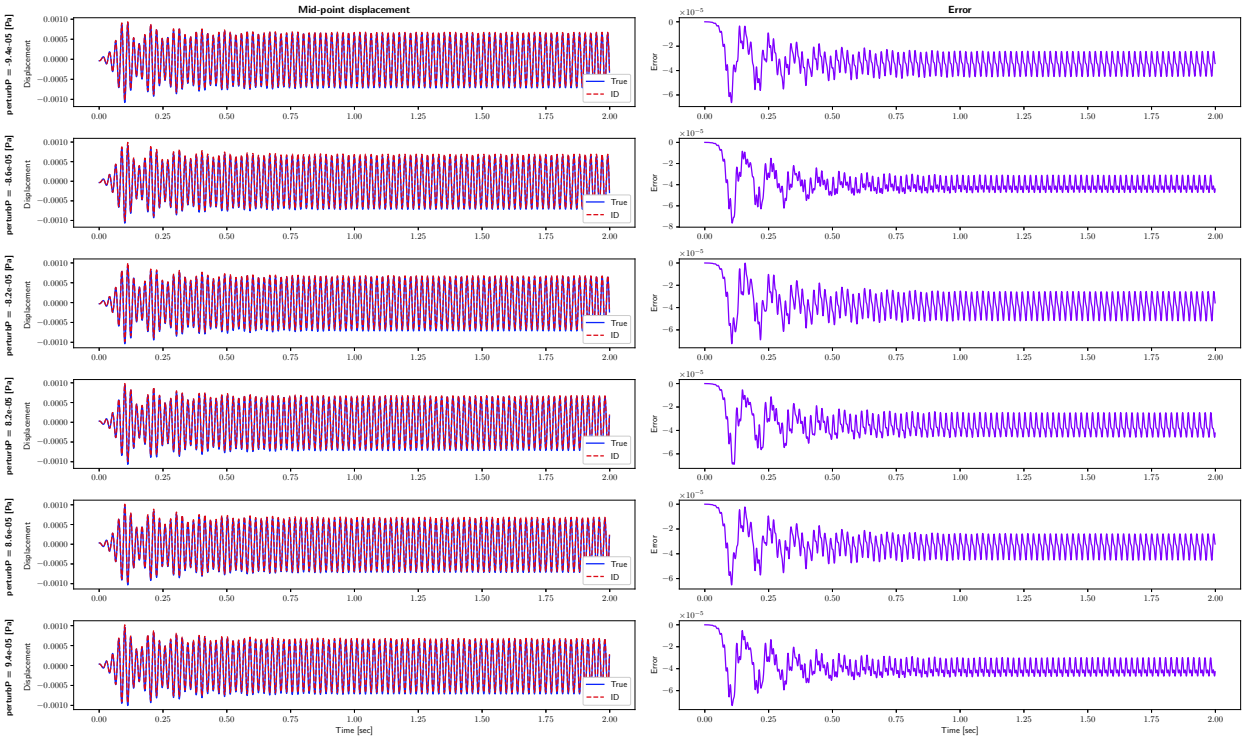

Fig. 9 Evolution of the mid-point displacement for six responses from the training set

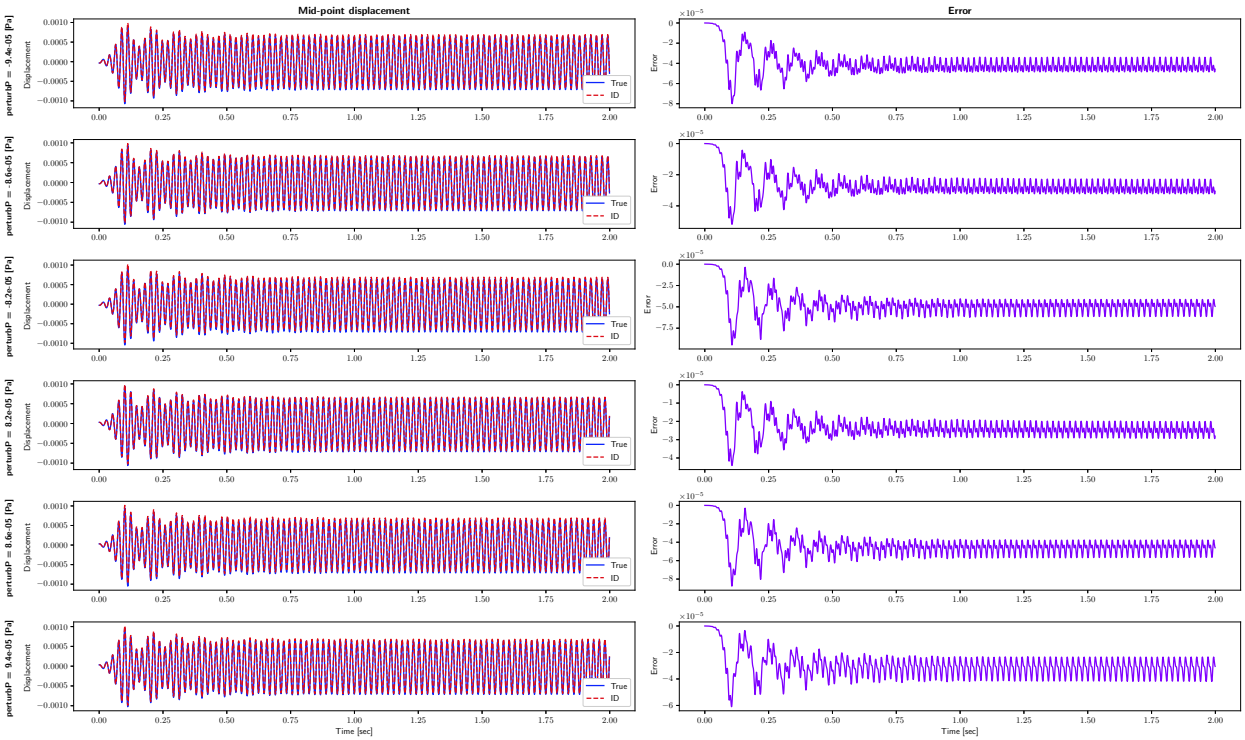

Fig. 10 Evolution of the mid-point displacement for six responses from the testing set

V. Conclusion

This work has presented a new time-varying identification method and its application to build a first-order approximation of a nonlinear dynamical system from repeated experiments. Specifically, the new algorithm is employed to generate reduced-order models of coupled thermal-structural responses for an academic panel flutter problem with time-varying thermal stress and a fully-coupled aerothermoelastic problem. The time-varying linear systems identified by the new algorithm were able to capture the nonlinear aerothermoelastic responses, including the limit cycle oscillations, with accurate reproduction of the amplitude, phase and frequency. The cases demonstrate the capability of the developed algorithm on a low order model where the measurements are of low dimension, as well as its generalizability to high-dimensional problems.

Towards practical aero-thermo-servo-elastic analysis of hypersonic vehicles, strong stochastic dynamics due to the atmospheric and aerothermal environments must be taken account of. The combination of time-varying versions of ERA and OKID (and also with data correlation) provides a viable means to tackle the challenge of uncertainty quantification in a nonlinear and high-dimensional system like the ATSE model. Specifically, it is possible to build the ROM of coupled thermal and structural response in a nominal ATSE simulation and couple the new thermoelastic ROM to the aerothermal model, so as to produce a computationally efficient linear time-varying ATSE model, which can be subsequently employed to study the departure dynamics of nonlinear ATSE response and perform uncertainty quantification of the ATSE responses over the entire trajectory of a hypersonic vehicle.

VI. Acknowledgment

This material is based upon work supported jointly by the AFOSR grants FA9550-17-1- 0088 and FA9550-20-1-0176.

References

[1] J. J. McNamara and P. P. Friedmann. Aeroelastic and Aerothermoelastic Analysis in Hypersonic Flow: Past, Present, and Future. AIAA Journal, 49(6):1089–1122, 2011.

[2] K. G. Bowcutt. Physics drivers of hypersonic vehicle design. In AIAA 2018–5373, 22nd AIAA International Space Planes and Hypersonics Systems and Technologies Conference, pages 1–22, Orlando, FL, Sept 2018.

[3] D. Huang. Development of a Hypersonic Aerothermoelastic Framework and Its Application to Flutter and Aerothermoelastic Scaling of Skin Panels. PhD thesis, University of Michigan, Ann Arbor, 2019

[4] M. E. Riley, R. V. Grandhi, and R. Kolonay. Quantification of modeling uncertainty in aeroelastic analyses. Journal of Aircraft, 48(3):866-873, 2011.

[5] B. Smarslok, A. Culler, and S. Mahadevan. Error quantification and confidence assessment of aerothermal model predictions for hypersonic aircraft. In 53rd AIAA/ASME/ASCE/AHS/ASC Structures, Structural Dynamics and Materials Conference, pages 1-13, April 2012.

[6] B. P. Smarslok and D. Villaneuva. Design of experiments for model calibration of multi-physics systems with targeted events of interest. Technical report, Hypersonic Sciences Branch, High Speed Systems Division, AFRL Wright-Patterson AFB, 2017.

[7] E. C. DeCarlo, B. P. Smarslok, and S. Mahadevan. Quantifying model discrepancy in time-dependent, coupled analyses. AIAA Journal, 56(6):2403-2411, 2018.

[8] N. Lamorte, P. P. Friedmann, B. Glaz, A. J. Culler, A. R. Crowell, and J. J. McNamara. Uncertainty propagation in hypersonic aerothermoelastic analysis. Journal of Aircraft, 51(1):192–203, 2014.

[9] B. P. Smarslok. Quantifying confidence in model predictions for hypersonic aircraft structures. Technical report, AIR FORCE RESEARCH LAB WRIGHT-PATTERSON AFB OH AEROSPACE SYSTEMS DIRECTORATE, 2015.

[10] A. J. Culler and J. J. McNamara. Impact of Fluid-Thermal-Structural Coupling on Response Prediction of Hypersonic Skin Panels. AIAA Journal, 49(11):2393–2406, 2011.

[11] N. J. Falkiewicz and C. E. Cesnik. Enhanced modal solutions for structural dynamics in aerothermoelastic analysis. Journal of Aircraft, 54(3):870-889, 2017.

[12] D. Huang and P. P. Friedmann. An aerothermoelastic analysis framework with reduced-order modeling applied to composite panels in hypersonic flows. Journal of Fluids and Structures, 2020.

[13] A. Forrester, A. Sobester, and A. Keane. Engineering Design Via Surrogate Modelling: A Practical Guide. John Wiley & Sons, 2008.

[14] Dowell, E. H., Aeroelasticity ofPlates and Shells, Vol. 1, Springer Science & Business Media, 1974. doi:10.1115/1.3423871.

[15] Gilbert, E. G. (1963) “Controllability and Observability in Multivariable Control Systems," SIAM Journal on Control, 1(2), pp. 128-151.

[16] Kalman, R. E. (1963) “Mathematical Description of Linear Dynamical Systems," SIAM Journal on Control, 1(2), pp. 152-192.

[17] Ho, B. L. and R. E. Kalman (1965) “Effective Construction of Linear State-Variable Models from Input/Output Data," Proceedings of the 3rd Annual Allerton Conference on Circuit and System Theory, pp. 449-459.

[18] Ho, B. L. and R. E. Kalman (1966) “Effective Construction of Linear State Variable Models from Input/Output Data," Regelungstechnik, 41(2), pp. 545-548.

[19] Juang, J.-N. and R. S. Pappa (1985) “An Eigensystem Realization Algorithm (ERA) for Modal Parameter Identification and Model Reduction," Journal of Guidance, Control, and Dynamics, 8(5), pp. 620-627.

[20] Juang, J.-N., Cooper, J. E., and Wright, J. R. (1988)“An Eigensystem Realization Algorithm Using Data Correlation (ERA/DC) for Modal Parameter Identification," Journal of Control-Theory and Advanced Technology, Volume 4, Number 1, pp 5-14.

[21] Juang, Jer-Nan, Horta, Lucas G., Belvin, W. Keith, Sharkey, John, Bauer, Frank H. “An application of the Observer/Kalman Filter Identification (OKID) technique to Hubble flight data," The Fifth NASA(DOD Controls-Structures Interaction Technology Conference, Part 1, February 1, 1993.

[22] Jer-Nan Juang, Minh Phan, Lucas G. Horta, and Richard W. Longman (1993) “Identification of Observer/Kalman Filter Parameters: Theory and Experiments," Journal of Guidance, Control, and Dynamics, 16(2), pp. 320-329.

[23] Cho, Y. M., Xu, G., and Kailath, T., “Fast Recursive Identification of State Space Models via Exploitation of Displacement Structure," Automatica, Vol. 30, No. 1, 1994, pp. 45-59.

[24] Shokoohi, S., and Siverman, L. M., “Identification and Model Reduction of Time Varying Discrete Time Systems," Automatica, Vol. 23, No. 4, 1987, pp. 509-521.

[25] Dewilde, P., and Van der Veen, A. J., “Time Varying Systems and Computations", Kluwer Academic, Norwell, MA, 1998, pp. 19-186.

[26] Verhaegen, M., and Yu, X., “A Class of Subspace Model Identification Algorithms to Identify Periodically and Arbitrarily Time Varying Systems," Automatica, Vol. 31, No. 2, 1995, pp. 201-216.

[27] Verhaegen, M., “Identification of Time-Varying State Space Models from Input-Output Data," in Workshop on Advanced Algorithms and their Realization, Bonas, 1991.

[28] Majji, M., Juang, J.-N., and Junkins, J. L., “Time-Varying Eigensystem Realization Algorithm," Journal of Guidance, Controls, and Dynamics, Vol. 33, No. 1, January-February 2010.

[29] Majji, M., Juang, J.-N., and Junkins, J. L., “Observer/Kalman-Filter Time-Varying System Identification," Journal of Guidance, Controls, and Dynamics, Vol. 33, No. 3, May-June 2010.

[30] Schmid, P. J., “Dynamic mode decomposition of numerical and experimental data," J. Fluid Mech. (2010), vol. 656, pp. 5-28.

[31] Jonathan H. Tu, Clarence W. Rowley, Dirk M. Luchtenburg, Steven L. Brunton, J. Nathan Kutz, “On dynamic mode decomposition: Theory and applications," Journal of Computational Dynamics, 2014, 1 (2) : 391-421. doi: 10.3934/jcd.2014.1.391

[32] Liu, K., “Identification of Linear Time Varying Systems," Journal of Sound and Vibration, Vol. 206, No. 4, 1997, pp. 487-505. doi:10.1006/jsvi.1997.1105